Materials Today Bio 28 (2024) 101247

Contents lists available at ScienceDirect

Materials Today Bio

journal homepage: www.journals.elsevier.com/materials-today-bio

Natural hydrogen gas and engineered microalgae prevent acute lung injury in sepsis

Yuanlin Wang [a,b,1], Qingqing Han [b,1], Lingling Liu [a,c,d,1], Shuai Wang [a,b], Yongfa Li [a,b], Zhanying Qian [e], Yi Jiang [a,**], Yonghao Yu [a,*]

[a] Department of Anesthesiology, Tianjin Medical University General Hospital, 300052, Tianjin, China
[b] The Graduate School, Tianjin Medical University, 300070, Tianjin, China
[c] Department of Anesthesiology, Tianjin Huanhu Hospital, Tianjin, 300350, China
[d] Tianjin Key Laboratory of Cerebral Vascular and Neurodegenerative Diseases Tianjin Neurosurgical Institute, Tianjin Huanhu Hospital, Tianjin, 300350, China
[e] Key Laboratory of Immune Microenvironment and Disease (Ministry of Education), The Province and Ministry Co-sponsored Collaborative Innovation Center for Medical Epigenetics, Tianjin Key Laboratory on Technologies Enabling Development of Clinical Therapeutics and Diagnostics (Theranostics), School of Pharmacy, Tianjin Medical University, Tianjin, 300070, China

ARTICLE INFO

Keywords:
Multi-omics
Sepsis related lung injury
Nano therapy
Molecular hydrogen
Chlorella vulgaris

ABSTRACT

Background: Hydrogen gas and microalgae both exist in the natural environment. We aimed to integrate hydrogen gas and biology nano microalgae together to expand the treatment options in sepsis.
Methods: Phosphoproteomics, metabolomics and proteomics data were obtained from mice undergoing cecum ligation and puncture (CLP) and inhalation of hydrogen gas. All omics analysis procedure were accordance with standards. Multi R packages were used in single cell and spatial transcriptomics analysis to identify primary cells expressing targeted genes, and the genes' co-expression relationships in sepsis related lung landscape. Then, network pharmacology method was used to identify candidate drugs. We used hydrophobic-force-driving self-assembly method to construct dihydroquercetin (DQ) nanoparticle. To cooperate with molecular hydrogen, ammonia borane (B) was added to DQ surface. Then, *Chlorella vulgaris* (C) was used as biological carrier to improve self-assembly nanoparticle. Vivo and vitro experiments were both conducted to evaluate anti-inflammation, anti-ferroptosis, anti-infection and organ protection capability.
Results: As a result, we identified Esam and Zo-1 were target phosphorylation proteins for molecular hydrogen treatment in lung. Ferroptosis and glutathione metabolism were two target pathways. *Chlorella vulgaris* improved the dispersion of DQB and reconstructed morphological features of DQB, formed DQB@C nano-system (size = 307.3 nm, zeta potential = −22mv), with well infection-responsive hydrogen release capability and biosafety. In addition, DQB@C was able to decrease oxidative stress and inflammation factors accumulation in lung cells. Through increasing expression level of Slc7a11/xCT and decreasing Cox2 level to participate with the regulation of ferroptosis. Also, DQB@C played lung and multi organ protection and anti-inflammation roles on CLP mice.
Conclusion: Our research proposed DQB@C as a novel biology nano-system with enormous potential on treatment for sepsis related acute lung injury to solve the limitation of hydrogen gas utilization in clinics.

1. Introduction

Sepsis is a life-threatening organ dysfunction caused by an imbalanced host response to infection. According to the latest Global Burden of Disease data from Lancet, the number of sepsis cases worldwide each year has exceeded 48 million, of which approximately 11 million patients die, with a mortality rate of over 20 % [2]. The American Society of Critical Care Medicine (SCCM) and the European Society of Critical Care Medicine (ESICM) jointly released the latest definition and diagnostic criteria for sepsis 3.0, emphasizing the research significance of valuing organ failure [3]. The latest guideline for sepsis management released by the European Society of Intensive Care Medicine also clearly

* Corresponding author. Department of Anesthesiology, Tianjin Medical University General Hospital, 300052, Tianjin, China
** Corresponding author.
E-mail address: yyu@tmu.edu.cn (Y. Yu).
[1] These authors have contributed equally to this work and share first authorship.

https://doi.org/10.1016/j.mtbio.2024.101247
Received 24 May 2024; Received in revised form 25 August 2024; Accepted 13 September 2024
Available online 14 September 2024

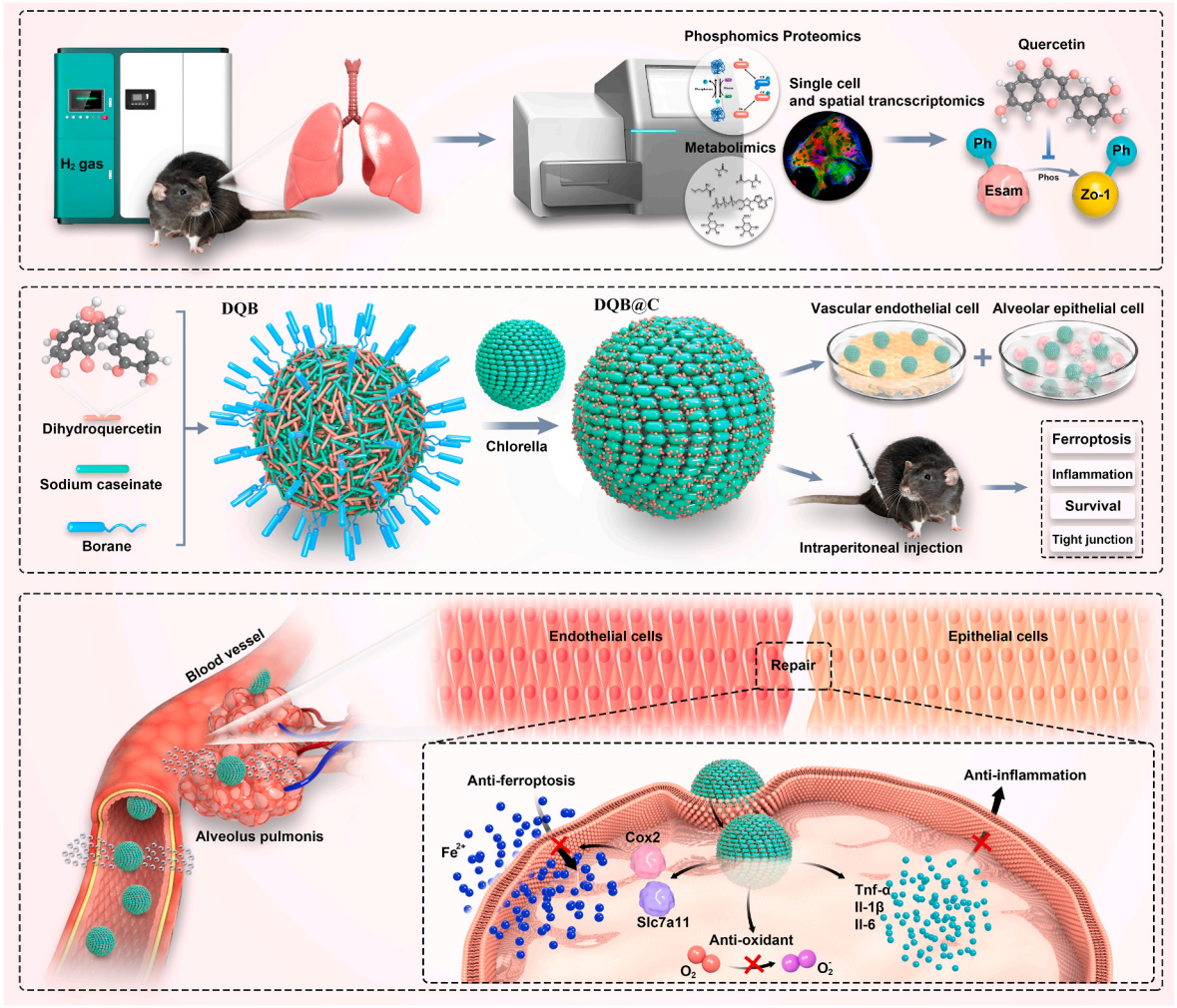

Fig. 1. Graphic abstract for this research. (i) Multi omics analysis could explore molecular hydrogen related molecule biology mechanism and potential natural drug collaborating with hydrogen gas. (ii) Methods of hydrophobic self-assemble could firstly construct self-assemble DQB nanoparticle carrying ammonia borane and dihydroquercetin. Utilizing the adsorption characteristics of algae for polyphenols, *Chlorella vulgaris* could establish a self-assembly nano system, DQB@C, to improve self-assemble of nanoparticle. (iii) Nano chlorella system is of better infection-responsive hydrogen and drug release capability. Vivo and vitro experiments proved anti-inflammation and organ protection ability of DQB@C.

states that the focus of treatment for sepsis patients is still on preventing and treating multiple organ dysfunction [4]. The most vulnerable organ to sepsis is the lungs, and acute respiratory distress syndrome can occur in severe cases. However, the pathogenesis of sepsis induced lung injury has not been accurately elucidated, and there is a lack of effective treatment methods.

Phosphorylation is the most important form of post-translational modification of proteins, involving almost all biological processes [5]. Phosphorylated proteins are involved and play important roles in sepsis related pathways [6–8]. The combination of single cell sequencing and spatial transcriptome can help us gain a more comprehensive understanding of gene expression regulation. Janosevic et al. used spatial transcriptomics combining with single-cell transcriptomics to establish a single-cell resolution gene expression profile for the progression of sepsis in mice. Spatiotemporal analysis identified biomarkers and targets, which can aid in staging and treating human sepsis [9].

At present, the understanding of the mechanisms of sepsis induced lung injury is mainly based on inflammation and oxidative stress [10–12]. However, the current treatment methods targeting these two mechanisms have limited effectiveness. Nanomaterials of natural products have shown great potential in resisting bacterial infections and treating inflammatory diseases [13,14]. Among them, self-assemble nano system based on natural products owned excellent antioxidant properties have attracted more attention. Dihydroquercetin is an excellent natural antioxidant. The ultra-small iron quercetin nano enzyme synthesized by Gui et al. solves the problems of poor solubility and low bioavailability, playing protective effects in inflammation and oxidative stress damage [15]. For dihydroquercetin, self-assemble method is also of potential to improve its effects on infection and inflammation treatment.

Our previous studies have shown that H_2 treatment significantly alleviates lung tissue pathological scores and oxygenation index in septic mice [16],and improves lung injury in septic mice by over activating the Nrf2/HO-1 signaling pathway [17]. But long-term inhalation of hydrogen gas can cause irritation to the respiratory mucosa and gastrointestinal tract, which has always been a concern for us. *Chlorella pyrenoidosa* is a single celled green alga belonging to the genus Chlorella in the phylum Chlorophyta. Previous studies have shown that it can produce hydrogen in the dark [18],and its cell wall has the function of carrying polyphenolic drugs. Chlorella has been used as a carrier in some studies to enable efficient expression of exogenous proteins [19–21]. What's more important, the vivo biosafety of Chlorella has gotten confirmed in many studies [22,23]. These make it suitable to collaboratively use with hydrogen gas. Ammonia borane (H_3N–BH_3, AB) is an excellent hydrogen storage compound [24]. Some studies utilized its ability to release hydrogen gas in acidic environments, hydrogen release

can be achieved in tumors and the stomach [25,26]. Infectious micro-environment in sepsis is also acidic [27], AB could release hydrogen gas in this condition.

This study revealed a new pathogenesis of sepsis induced lung injury by combining phosphoproteomics, single-cell and spatial transcriptomics, metabolomics, and provided a therapeutic method and basis for nanocellulose loaded drugs in sepsis induced lung injury.

2. Materials and methods

The flow of all the experiments is shown in Fig. 1.

2.1. Samples acquisition and phosphoproteomics assay

Mice model of severe sepsis was successfully constructed using the cecum ligation perforation (CLP) method. Adult male C57BL/6J mice, weighing 20–25 g were bought from Laboratory Animal Center at the Hygiene and Environmental Medicine Institute of the Military Medical Science Academy for constructing model. To conduct operation, male C57BL/6J mice were anesthetized with sevoflurane, and the abdominal cavity was incised under aseptic conditions. The abdominal cavity was incised under aseptic conditions using sevoflurane anesthesia, and the cecum was gently pulled out and ligated at the distal 2/3 of the cecum. To promote the development of inflammation, small amount of feces were specially squeezed out, then cecum was retracted into the abdominal cavity, sutured abdominal wall. To proceed resuscitating, 37 °C saline was injected subcutaneously (5 ml/100g) to mice neck. Details of the procedure were referred to the published articles of our group [28].

Mice belonging to the group accepting molecular hydrogen treatment were placed in a sealed Plexiglas box, hydrogen gas and nature air were mixed through a gas meter. After mixing, gas was fed into the box through the inlet port. H2Scan, Valencia, CA, USA) was used to measure the hydrogen concentration (to maintained at 2 %), as well as the oxygen and carbon dioxide levels in the chamber. The control group, which was not treated with hydrogen, was simply placed in the same environment without hydrogen treatment. The control group without molecular hydrogen treatment was simply placed in the same environment without hydrogen treatment.

For phosphorylation proteomics assay, abbreviated workflow was below: 1. Sample Whole Protein Extraction; 2. proteolytic cleavage to peptides; 3. Peptide desalting; 4. Enrichment of acidified peptides; 5. Q-exactive analysis; 6. Qualitative and quantitative proteomics results; 7. get the relative quantitative ratio of proteins to their quantification in different samples.

2.2. Metabolomics detection

After the lung sample was thawed slowly at 4 °C, an appropriate number of samples were added to pre-cooled methanol/acetonitrile/water solution (2:2:1, v/v), vortexed and mixed, and then sonicated at low temperature for 30 min. Then, allowed to stand at −20 °C for 10 min, and centrifuged at 14,000 g for 20 min. For mass spectrometry analysis, added 100 μL of acetonitrile aqueous solution (acetonitrile: water = 1:1, v/v), vortex, centrifuge at 14000 g for 15 min at 4 °C, and toke the supernatant into the sample for analysis.

The samples were separated on an Agilent 1290 Infinity LC ultra high performance liquid chromatography (UHPLC) column. The AB Triple TOF 6600 mass spectrometer was used for the acquisition of primary and secondary spectra of the samples.

The raw data were converted to mzXML format by ProteoWizard, and then XCMS software was used for peak alignment, retention time correction, and peak area extraction. XCMS extracted data and firstly subjected to metabolite structure identification and data preprocessing, followed by experimental data quality evaluation and finally data analysis.

2.3. Bioinformatics analysis for phosphoproteomics assay

2.3.1. Clustering analysis

To assess the data quality and distribution of phosphoproteomics data, we performed clustering analysis through R studio software based on R language.

2.3.2. Quantitative analysis of differential phosphorylated protein

The results of PRM (Parallel Reaction Monitoring) mass spectrometry were analyzed via Skyline quantitative analysis, and expression information of the target peptides in each sample were obtained after signal correction of the internal standard peptides. Then, after signal correction, the expression amounts of the target peptide in each sample were obtained. Further, statistical analysis was conducted to identify differential expression of target proteins in different groups of samples.

In addition, due to the existence of modified proteins with multiple phosphorylation sites and different down-regulation trends at different phosphorylation sites. It is impossible to perform quantitative analysis at the level of modified proteins, and thus the phosphorylated peptides were analyzed for differential expression analysis. The phosphorylated peptides with a fold change of more than 2-fold (up-regulation of more than 2-fold or down-regulation of less than 0.5-fold) and a *p-value* of less than 0.05 were screened. Phosphorylated peptides screened with a fold change of more than 2-fold (up-regulation of more than 2-fold or down-regulation of less than 0.5-fold) and a *p-value* of less than 0.05 were considered to be differentially expressed. We screened candidate peptides and proteins according to the criteria: molecular hydrogen could reverse the expression change induced by sepsis. Venn diagram method (http://jvenn.toulouse.inra.fr/app/example.html) was used to screen common phosphorylated sites and proteins.

2.3.3. GO and pathway analysis

Blast2Go software was used to annotate the Gene Ontology (GO) function of all proteins identified as differentially expressional proteins. Then the GO function enrichment analysis of proteins corresponding to differentially expressional phosphorylated peptides was performed. Total three species of functions were included, CC (cellular component), BP (Biological process), Molecular function (MF), to reveal the biological function change among different groups.

For pathway analysis, we used Kyoto Encyclopedia of Genes and Genomes (KEGG) database to evaluate enrichment pathway of above canadiate proteins. R package ggplott2 was used to exhibit the results. We specially focused on the differential enrichment of pathways among different groups.

2.3.4. Protein-protein-interaction network construction

String database was used to construct the protein-protein-interaction (PPI) network of canadiate proteins. Cytoscape software helped visualize the network. The importance status of proteins were sorted according to degree, an index indicating the amounts of proteins interacting with certain protein.

2.4. Bioinformatics analysis for metabolomics

2.4.1. Principal component analysis

Principal Component Analysis (PCA) is an unsupervised data analysis method that reorganizes all metabolites originally identified into a new set of composite variables. Thus, the purpose of dimensionality reduction was achieved. At the same time, principal component analysis of metabolites can also reflect the variability between and within sample groups in general. Therefore, in the data analysis, the PCA method was generally used first to observe the overall distribution trend of the samples between groups and the degree of variability of the samples between groups.

2.4.2. Univariate statistical analysis

Univariate statistical analysis method is one of the most commonly used statistical analysis methods. Based on univariate analysis of variance, all metabolites detected in positive and negative ion modes (including unidentified metabolites) were analyzed for differences. FC > 1.5 or FC < 0.67, *p-value* < 0.05 for differential metabolites. Then, volcano plot was used to exhibit differential metabolimits positive ionization mode and negative ionization mode. Based on the species of metabolimites, heatmap also helped exhibit these differential metabolimites.

2.4.3. Pathway analysis for KEGG and differential metabolisms

We used Database forAnnotation, Visualization andIntegratedDiscovery (DAVID) database to identify metabolic pathway related with metabolites. Criteria for important pathways was: *p-value* $<$ 0.05. Rstudio software was used to draw dotplot of these pathways.

2.5. Data acquisition of single cell, mRNA transcriptomes and spatial transcriptomics

We downloaded single cell dataset matrix from GEO database, GSE207651, to analyze gene expression changes in lung after CLP operation. For spatial transcriptomics, GSE202322 was acquired from database. This dataset included mice samples owning pneumonia induced by influenza A virus. We used these the two types of mice models for furtherly evluating phosphorylation genes change.

2.6. Preprocessing and quality control of single cell

R package Seurat was utilized to conduct preprocessing procedure. Only cells and genes were in accordance with below criteria would be adapted to next: genes which at least expressed in three cells, cells which were capable of detecting two hundred genes. In contrast, those not satisfied would be abandoned. Decise data quality control was based on mitochondrial proportions, cells containing from 200 to 2500 genes and within not more than five percent mitochondrial genes were retained for next analysis. In addition, data normalization and mutation genes screening were performed to decrease the possibilities of potential error rate arising caused by a great amount of low-quality cells. Then, to distinguish cells with different clusters referring to gene expression, principal componet analysis (PCA) algorithms were performed. At last, the visualization was realized via tSNE agrithms, exhibiting the cells' distribution situation in two-dimension level.

2.7. Cell type identification and genes distribution detection

Cell markers used to identify cell types mixed in single cell matrixes were originated from Cell Marker2.0 database (http://bio-bigdata.hrbmu.edu.cn/CellMarker) [29] and previous literature or researches. Firstly, distribution of phosphorylation genes was marked in single cell landscape to find the most important cell type being of relationship with these genes. Then, extracted the phosphorylation related cells to observe the expression relationships between three inflammatory genes (Tnf,Il1 and Il6) and phosphorylation genes. In the cluster of phosphorylation related cells, we separarted cells according to the expression level of Tjp1 genes. Cells, which of higher expression were named as higher expression group, others were medium expression group or lower expression group.

2.8. Analysis of spatial transcriptomics

R package Seruat and hdf5r, patchwork were utilized to deal with spatial transcriptomics data. The spatial distribution of gene and cell type were also realized. We aimed to explore the gene expression change and coloacalization relationship in both control and pneumonia group.

2.9. Candidate drug screening

We used drug database, HERB [30], a high-throughput experiment- and reference-guided database of traditional Chinese medicine. By importing list of genes encoding proteins into database, we searched promising medicine herbs targeting these proteins. Common herbs among these candidates were then identified.

2.10. Construction of Chlorella pyrenoidosa carrying self-assemble nanoparticle

We obtained *Chlorella pyrenoidosa* from *Chinese Academy of Science*, Dihudrogquercetin was obtained from shycbio company.To improve the solubility of DQ, we increase the temperature to 70 °C, the conceration of DQ in water was 5 mg/ml. Then, sodium caseinate was added, ratio of mass was 1:1, as emulsifiers and stabilizers. Cell crusher instrument which could produce ultrasound, at 70w for 7min. Meanwhile, temperature was decreased to 0 °C. Self-assemble DQ nanoparticle was created. Then, according to mass ratio 5:1 (dihydroquercetin and ammonia borane), ammonia borane was added to DQ self-assemble system. The final concentration for DQ was 11 mg/ml. Low temperature ultracentrifuge was used to extract *Chlorella pyrenoidosa* from medium mixtrure environment. Counting 1×10^7 logarithmic growth phase *Chlorella pyrenoidosas* to add into 1 ml DQB nanoparticle systems. After placing on magnetic stirrer, the temperature was kept at 30 °C, the stirring speed was 400r/min. Overnight, nano microalgae system, DQB@C, was achieved.

2.11. Detection of physical and characters of DQB@C

Dynamic light scattering techniques were used to detect zeta potential and particle size of DQ, DQB and DQB@C nanoparticle. Then, we used electron microscopy to observe the morphology of DQB@C and DQB. By marking DQB with propidium iodide (PI), and colocating within microalgae, we used fluorescence microscopy and flow cytometry analyzer to detect the adsorption of DQB by microalgae [31,32]. Then, hemolysis experiment was performed to evaluate vivo biostability. And we detected the cell toxiology for two cell types, Human Umbilical Vein Endothelial Cells (HUVECs) and Human lung (bronchial) epithelial cells (BEAS-2B), through Cell Counting Kit-8 (CCK8). The set treatment concentration referred to dihydroquercetin, (from 0 μg/ml to 100 μg/ml). We used microelectronals (Unisense company) to detect the hydrogen release speed and vivo inflammation organ hydrogen concentration in CLP mice [25,33]. To detect the hydrogen production and release ability of nano system in simulating infection-environment, we modulated PH to 6.5. In vivo, conducted intraperitoneal injection of 200 μL DQB@C in CLP mice and we tracked hydrogen gas concentration changes in infectional organ. Due to lung could not be fixed in living state, so we detected liver.

2.12. Cellular uptake assay detection and chlorella phagocytosis observation

Two types of cells in lung, BEAS-2B and HUVECs, were both used in cell level. DQB@C was cocultured with cells (20 μg/ml, referred to concentration of dihydroquercetin). Then, immunofluorescence microscopy observed the fluorscence density change at different timepoints. Dil membrane dye was used to mark cell membrane. Processes of dynamic phagocytosis by cells were tracked under immunofluorescence microscopy.

2.13. Oxidative stress detection and ELISA, ferroptosis evaluation

Five groups were included in vitro experiments, including normal group, lipopolysaccharide (LPS) stimiulating group, LPS + hydrogen water group, LPS + DQB group, LPS + DQB@C group. When the cell

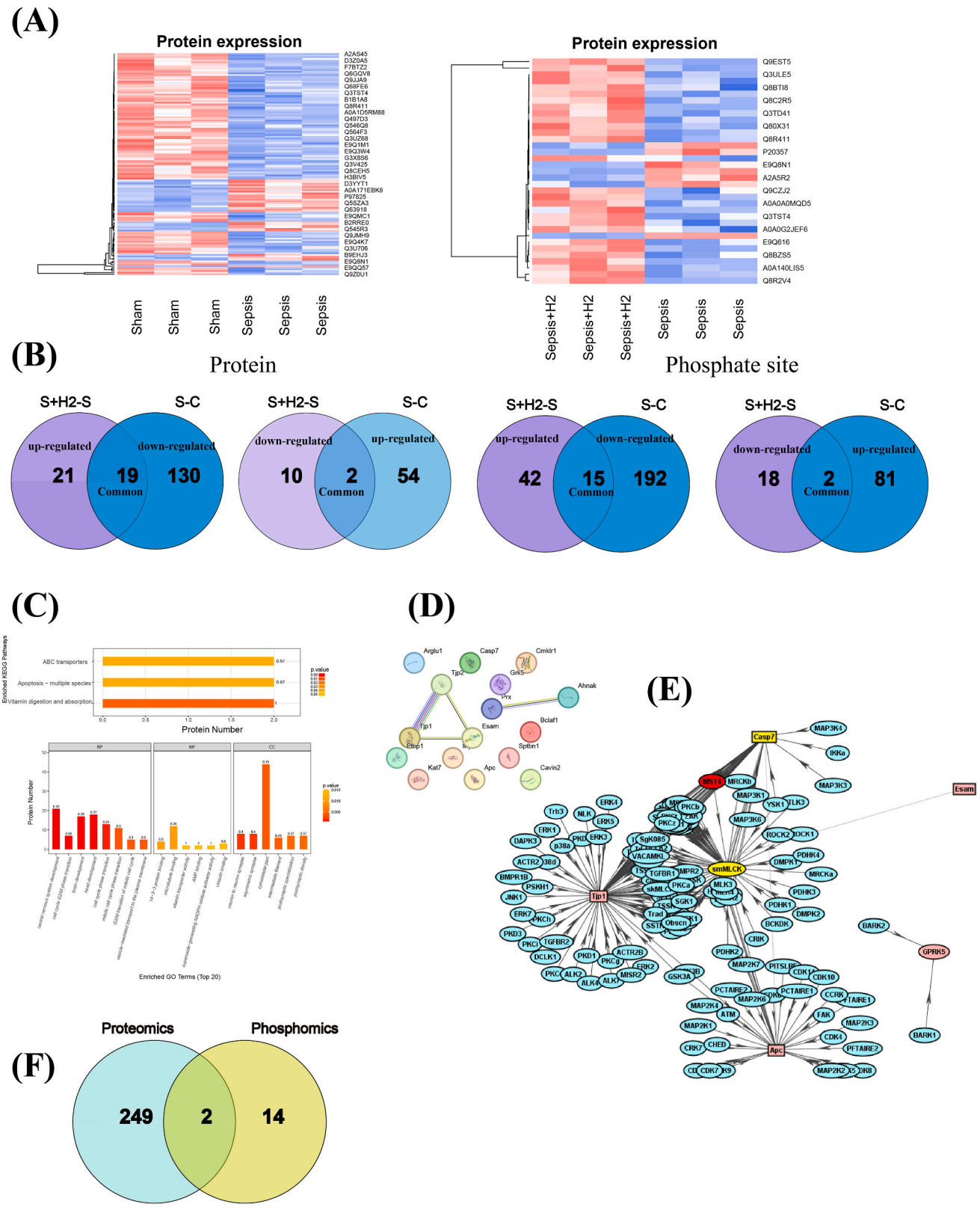

Fig. 2. Results for phosphoproteomics and proteomics integrative analysis. (**A**) Heatmap distribution of top differentially expressional phosphorylated proteins between sepsis, control and hydrogen; Red exhibited high expression and blue represented low expression. (**B**) Venn diagram for molecular hydrogen related phosphate site and proteins. The criteria were: molecular hydrogen enable to reverse expression changes induced by sepsis. (**C**) KEGG and GO pathways for hydrogen related phosphorylated proteins. (**D**) PPI network for molecular hydrogen related phosphorylated proteins. Dots represented protein, lines presented that the relationship among proteins. (**E**) Kinase substrate network of hydrogen related phosphorylated proteins. The protein emitting the arrow is the kinase and the protein pointing is the substrate **(F)** Common proteins between proteomics and phosphomics. Turquoise represented protein screened in proteomics, yellow represented protein screened in phosphomics. (For interpretation of the references to colour in this figure legend, the reader is referred to the Web version of this article.)

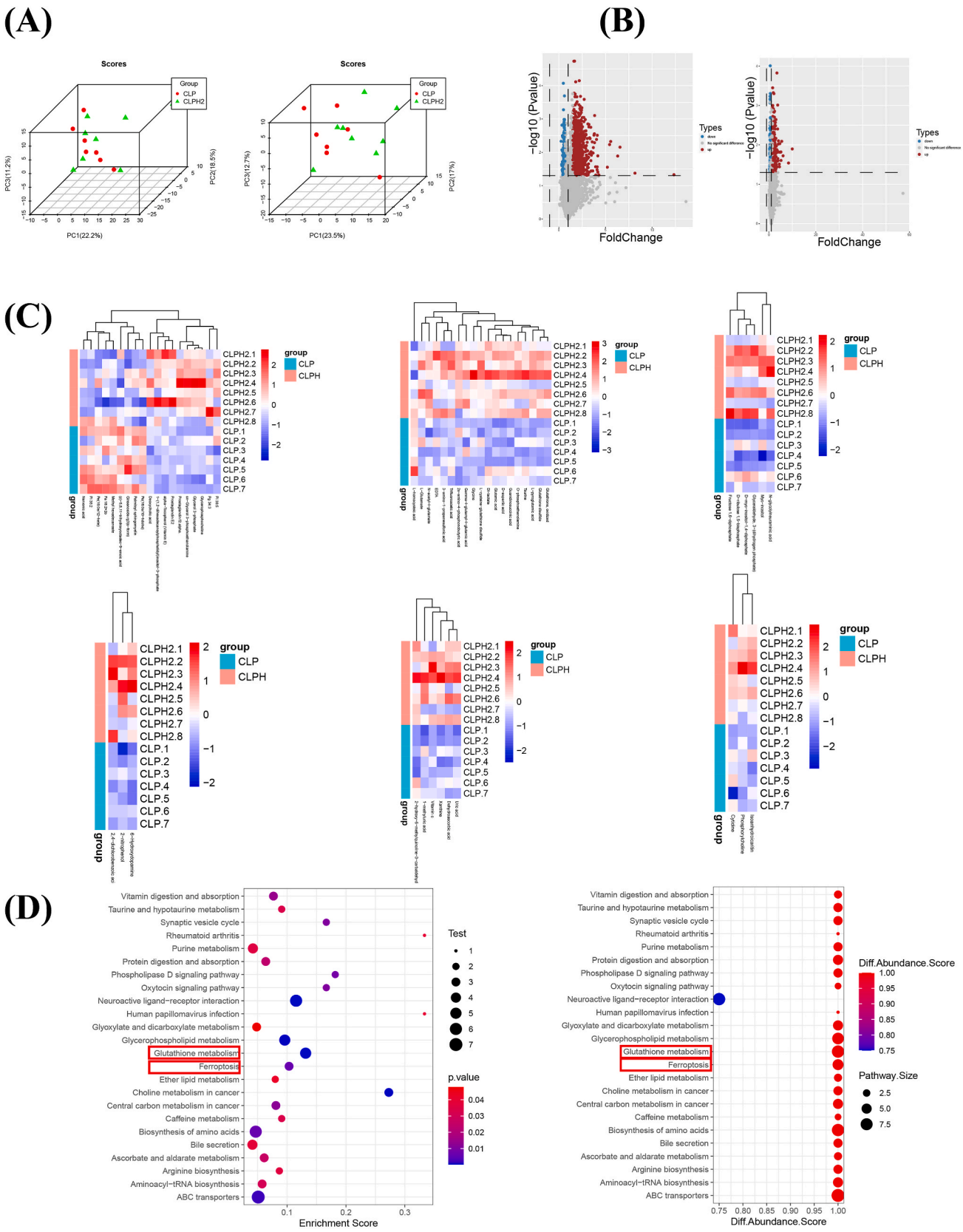

Fig. 3. Bioinformatics analysis for metabolomics results. (A) Spatial principal component analysis distribution for samples; different colors represented different groups; **(B)** Differentially metabolites in two modes; blue = down, grey = no significant difference, red = up; **(C)** Top differential metabolites in different groups; **(D)** Dot plots of KEGG pathways and differ abundances. The color of dot represented *p-value* and abundance scores. The size represented numbers of metabolites. (For interpretation of the references to colour in this figure legend, the reader is referred to the Web version of this article.)

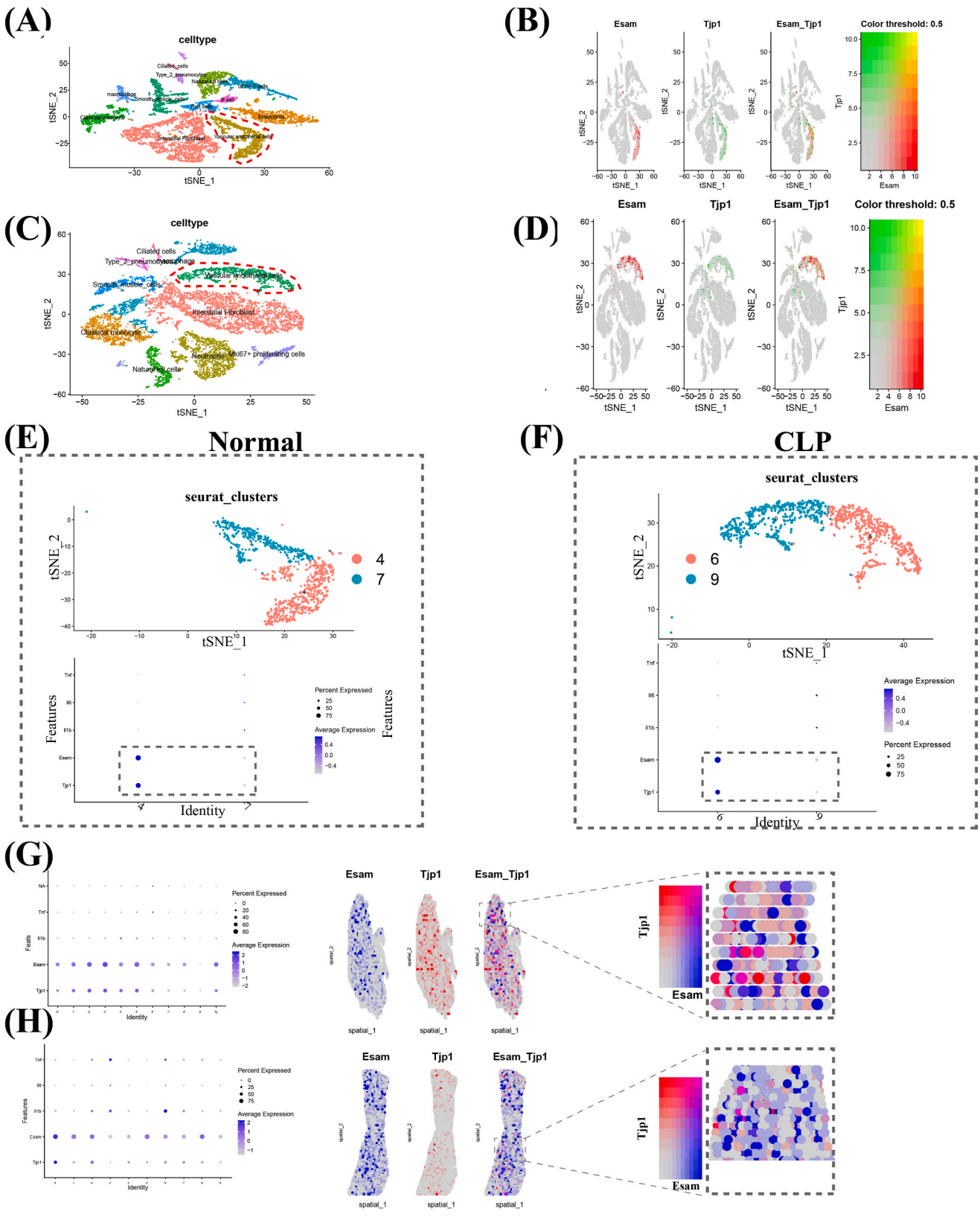

Fig. 4. Spatial and single cell integrative transcriptomics analysis. (A, B) Cell landscape and two genes colocalization landscape of normal lung. The region marked by red dotted line was two genes high expression cell cluster. **(C, D) C**ell landscape and two genes colocalization landscape of CLP lung. The region marked by red dotted line was two genes high expression cell cluster. (**E**) Cell landscape of expressing two genes in normal vascular endothelial cell cluster. Respectively scattered point and tSNE landscape. (**F**) Cell landscape for expressing two genes in CLP vascular endothelial cell cluster. Respectively scattered point and tSNE landscape. **(G, H)** Spatial colocalization of two genes in normal and pneumonia lung tissues. Red to blue color represented the gene expression status in spatial dots for two genes, Tjp1 and Esam. (For interpretation of the references to colour in this figure legend, the reader is referred to the Web version of this article.)

grows to a density of 50 %, respectively 100 μg/ml LPS and 10 μg/ml LPS started to stimulate HUVECs and BEAS-2B, lasting for 24 h. Methods for creating hydrogen-rich water medium (HW) were referred to our previous study [34]. All vitro treatments initiated simultaneously with LPS stimulation. For treatment dosage of DQB and DQB@C, both were 20 μg/ml (referred to concentration of dihydroquercetin). Dihydroethidium (DHE) could detect intracellular superoxide anion levels. We obtained DHE dye from Aladdin company. 50 μM DHE was incubated with cells and then fixed. In addition, DCFH-DA probe (Solarbio company) was used to detect reactive oxygen species (ROS), indirectly revealing changes of glutathione metabolism. Dynamic detection of intracellular Fe^{2+} concentration changes was also realized through Ferroorange probe (Servicebio company). Mitochondrial status change is also essential for ferroptosis, tracking this change could help evaluate effects of DQB@C. JC1 probe (Solarbio company) was used. In addition, we quantified the inflammatory factor secretory levels of two cells in five groups. For both HUVECs and BEAS-2B, IL-6 is the primary secreted factor [35]. Meanwhile, we detected Tnf-α and Il-1β level to validate their relationship with Zo-1 and Esam. Then, two promary ferroptosis markers, anti Cox2 antibody (ab179800) and anti Slc7a11/xCT antibody (ab307601), were used to conjunct with proteins. We used fluorescence detection to observe changes of intracelluar protein expression level.

2.14. Western blot

To quickly lyse cells, RIPA buffer (Sigma R0278) was used in HUVECs and BEAS-2B to extract protein from five groups. Add phenylmethylsulfonyl fluoride meanwhile to inhibit protein degradation. Following bicinchoninic acid method and electrophoresis, membrane transfer, protein closure procedures were all accordance with standard. After primary antibody incubation (anti-Zo-1 antibody (bs-34023R), anti-Esam antibody (bs-5838R), and anti-β-actin antibody (ab8226)), secondary antibody from Abcam company was used to bind with primary antibody.

2.15. Vivo anti-inflammation and organ protection effects evaluation

CLP mice model was constructed as **2.1**. At post-operation 1 h and 6 h timepoint, 100 μL DQB@C or DQB were injected into abdominal cavity. For CLP + meropenem group, meropenem (4 mg/kg) was dissolved into saline and injected after CLP operation. Five groups were adapted in vivo experiments: Sham, CLP, CLP + DQB, CLP + DQB@C, CLP + meropenem. 24 hour survial rate was recorded. To evaluate systemitic inflammation and multi organ function, serum was used to detect aminotransferase (ALT), creatinine, C reactive protein (CRP), surfactant-associated protein D (SP-D) and soluble receptor for advanced glycation end products (sRAGE) through ELISA Assay Kit. Besides, respectively 50 μL blood extracted from four groups (sham, CLP, CLP + DQB@C, CLP + meropenem) were used for plat blood bacterials culture to evaluate anti-infection effects. Then, we extracted important organs, including heart, liver, lung, kidney and spleen for H&E staining. Acute lung injury was our focus, thus, protein expression changes of two target proteins, Zo-1 and Esam in lung tissue sections was observed through immunofluorescence. And we used tissue Fe^{2+} content assay kit (AKIC001M), glutathione (GSH) Assay Kit (KGA7305-100), Malondialdehyde Assay (MDA) Kit (S0131S) to detect iron and antioxidants level in lung tissue.

2.16. Statistical analysis

Using ImagJ software to quantifiliy measure fluorescence intensity. Origin software and GraphPad Prism 10.1.2 software were used to perform statistical analysis. We used one-way ANOVA test to analyze group data. Statistical significance is identified as: $p\text{-value} < 0.05$.

3. Results

3.1. Differentially phosphorylation proteins and pathway analysis

In Fig. 2A, we identified differentially expressional phosphorylation proteins and sites, respectively between sepsis and normal, sepsis and sepsis after hydrogen gas inhalation. Then, to preciesely position to phosphorylation sites, we used same Venn diagram methods as above to screen (Fig. 2B). And, corresponding proteins for molecular hydrogen targeting phosphorylation sites were then compared with above proteins to find the key proteins. Totoal twenty phosphorylation sites and seventeen phosphorylation proteins were screened. Respectively for two differentially expressional proteins clusters, spesis-molecular hydrogen and sepsis, sham and sepsis, enriched pathways were exhibited in Fig. 2C. Then, we identified sixteen common proteins in two clusters (supplementary materials Fig. 1S).Among them, we identified phosphorylation sites, S(1)VAS(1)S(1)QPAKPTK in Zo-1 and MGAVPVMV-PAQS(1)QAGS(1)LV, in Esam as candidate. Three pathways, vitamin digestion and absorption, apoptosis - multiple species and ABC transporters were thought to be of significance between sepsis and sepsis with molecular hydrogen group. Among them, ABC transporters is a type of metabolic pathway. It is also related with ferroptosis we focused [36].

In PPI network, Fig. 2D, we found Tjp1-Tjp2-Esam network located on the centre, linking with other proteins, suggesting its primary roles in the phosparylation of molecular hydrogen participated.

In addition, by importing these proteins into iGPS, we acquired the kinase-substrate networks for differentially expressional phosparylation proteins Fig. 2E. Three interations were identified in network, smMLCK-Casp7, Apc- Casp7, Esam-Tjp1. These were three pairs of kinase-sunstrates. Consistently, Tjp1-Esam pair was also identifed. We also used previous lung proteomics data to identify common proteins [37], Fig. 2F, Zo-1 was screened. Above all, in differentially expressional analysis, phosparylation sites of Tjp1 were down-regulated after molecular hydrogen treatment, indicated the restore of substrate. In contrast, phosparylation sites expression level of Esam was up-regulated, suggested the activation of kinase.

3.2. Results for metabolomics

In Fig. 3A, two groups enabled to be separated independently, indicating that differences between CLP and molecular hydrogen treatment after CLP were significant. Then, we respectively exhibited differentially metabolites in POS and NEG mode (Fig. 3B). Total 1045 and 636 species of metabolites in NEG and POS were identified. According to main class of metabolites, lipids and lipid-like molecules; alkaloids and derivatives; benzenoids; nucleosides, nucleotides, and analogues; organic acids and derivatives; organic nitrogen compounds; organoheterocyclic compounds; phenylpropanoids and polyketides, and undefined, the distribution in samples of top differential metabolites were exhibited in Fig. 3C. Following pathway analysis, Fig. 3D, suggested that ferroptosis and glutathione metabolism pathway were enriched and of differential abundance. So, further experiments will also focus on these.

3.3. Gene localization of Tjp1 and Esam in single cell analysis

We identified distributions of nine celltypes in lungs, nature kill cells, neutrophil, mki67+ proliferating cells, smooth muscle cells, macrophage, vascular endothelial cells, classical monocyte and interstitial fibroblast, ciliated cells in Fig. 4A and C. The co-localization of two genes in CLP and sham mice lung were assessed. We could observe most high expression Tjp1 and Esam mRNA were enriched in vascular endothelial cells (Fig. 4B and D). So, extracted vascular endothelial cells for further analysis. In Fig. 4E and F, respectively two clusters in vascular endothelial cells cluster were identified in both CLP and normal lung. Interestingly, the expression change of Esam and Tjp1 was

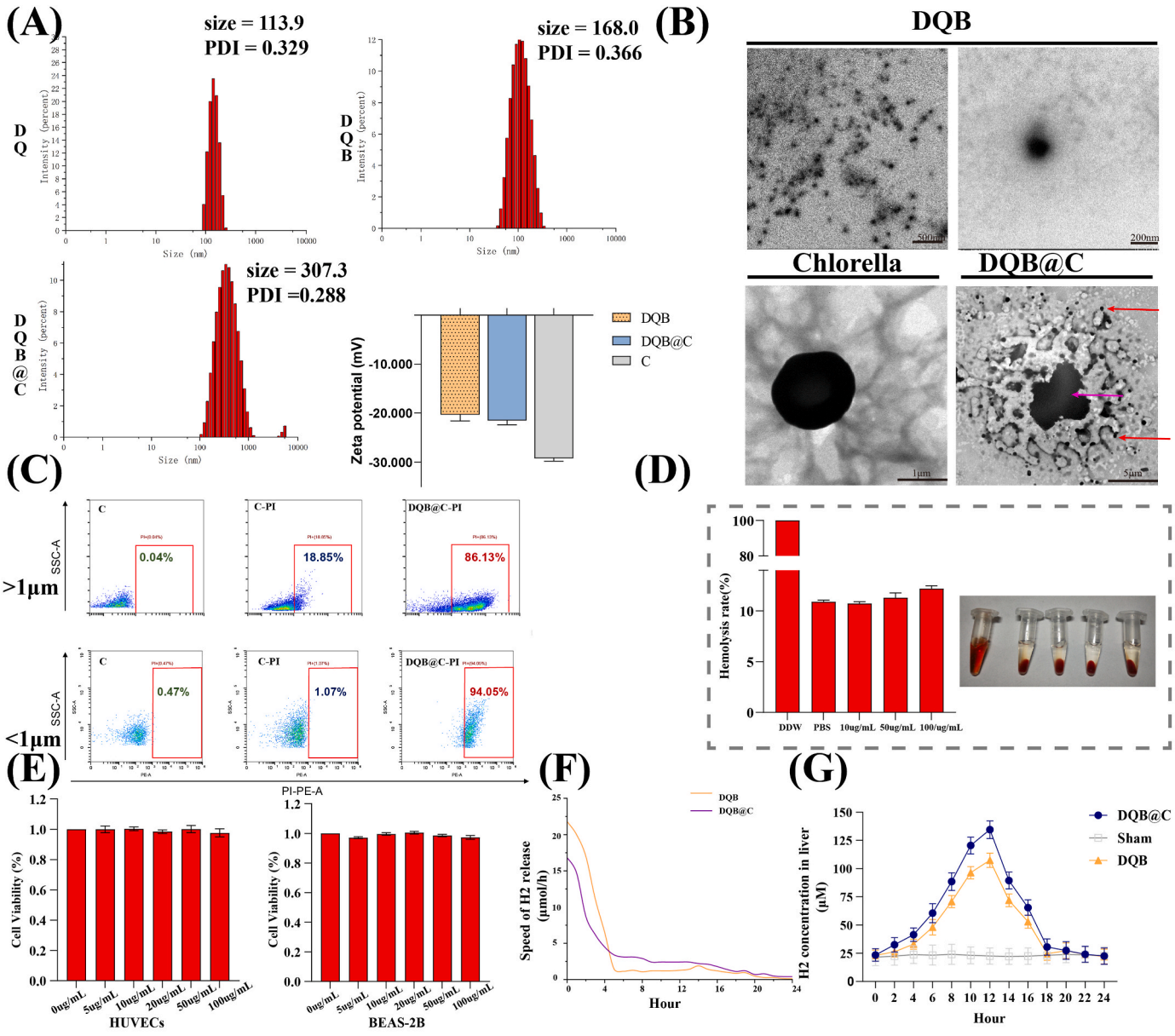

(caption on next page)

Fig. 5. Construction of DQB@C nano system and intracellular uptake detection. (A) Particle size and zeta potential distribution plot; different colors represented different nanoparticles in zeta potential bar chart. (**B**) TEM image for DQB, Chlorella and DQB@C; red arrow points to DQB, pink arrow points to Chlorella. (**C**) Flow cytometry distribution maps of DQB@C by PI staining. >1 μm: represented those particles whose size larger than >1 μm <1 μm: represented those particles whose size smaller than >1 μm. The particles inside the red box are PI positive. (**D**) Statistical chart of vitro nano-system hemolysis rate. (**E**) Cell viability for HUVECs and BEAS-2B in different DQB@C concentration; (**F**) 24 h hydrogen gas release speed curve of DQB@C and DQB in simulating infection-microenvironment (200 μL DQB and 200 μL DQB@C). (**G**) 24 h vivo hydrogen gas concentration curve after DQB@C injection (200μLDQB and 200 μL DQB@C). **(H)** Fluorescent image for intracellular absorption of DQB@C. From 0 h to 12 h, 24 h. Green represented nanoparticles absorbed by cells. Red represented cell membrane. Blue represented cell nucleus. Scale bar, 40 μm. All bar graphs are expressed with mean ± SD, n = 5. (For interpretation of the references to colour in this figure legend, the reader is referred to the Web version of this article.)

consistent, meanwhile highly expressed in one cell cluster and lowly in another. We also observed the down-regulated expression of Tjp1 and Esam accompanied with high-regulated expression of inflammation genes, Tnf, Il-1b and Il-6. This indicated that inflammation endothlial cells expressed less Tjp1 and Esam mRNA.

3.4. Co-localization of two genes in spatial transcriptomics

In Fig. 4G and H, we compared the spatial co-localization of two genes between virus infecting lungs and normal lungs. We could observe large amounts of co-high expression spatial locatizations were existed in lungs before and after virus infected. Nine days after virus infected, the expression levels of Tjp1 and Esam were both downregulated. In addition, inflammation genes high expressional zones were of lower Tjp1 and Esam expression level. These indicated that co-expression of two genes was obvious and infection could down-regulate their expression level in spatial dimension of lung.

3.5. Target plant medicine ingredients for Esam and Tjp1

Three integredients, 3,4-benzopyrene, meletin and querctin, were screened for Esam. Sixteen integredients were screened for Tjp1. Common integredient was querctin (supplementary materials Table1s). So, dihydroquercetin, as structural analogues of querctin being of more phenolic hydroxyl groups, was used for following nano therapy.

3.6. Construction of Nano-Chlorella vulgaris

Firstly, we built nano-chlorella pyrenoidosa carrying borane and dihydroquercetin. By self-assembling, the DQ nanoparticle was approximately 113.0 nm (Fig. 5A). The junction of borane with DQ was depended on polar interaction among mcromolecules. Size enabled to arrive 168 nm after complexed with borane. Whereas the completed self-assembly of DQB was insufficient and lacks good dispersibility. Cell wall of *Chlorella pyrenoidosa* was composed of polysaccharide structures, of ability to absorb polyphenols like dihydroquercetin. As the absorption of microalgae with DQB, the self assemble system of DQB got improved. And we can observe surface zeta potential of *Chlorella* was changed due to adhension of DQB (Fig. 5A). Size of final nano-system was nearly 300 nm. In Fig. 5B, TEM detection revealed that mere DQB system was easy to gather, the stability was bad. While, DQB@C nanao system was of better dispersibility. And DQB@C nanoparticles was absorbed to the surface or around *Chlorella*. This is helpful to quickly release nanoparticles as the inflammation microenvironment occurred. We also detected the autofluorescence of *Chlorella pyrenoidosa* to assess live situation. Under the acitivating threshold of FITC, green fluorescence was aboserved, indicating the integrity of the structure (supplementary materials Fig. 2S). PI not enabled to come into live cells, while, in PI activating light threshold, overlapping of red marker PI with microalgae suggested the conjunction of DQB nanoparticle. Furthermore, flow cytometry helped quantify the carrier ability of *Chlorella pyrenoidosa* for DQB. In Fig. 5C, we primarily focused on two species of DQB@C nano system, smaller than 1000 nm and larger than 1000 nm. According to our results, the PI absorbation rate increased significantly after wrapped by DQB. For smaller DQB@C, the rate ranged from 1.07 % to 94.05 %. In fact, this part represented DQB. This indicated DQB was able to be coupled with PI. In larger DQB@C system, the rate increased from 18.85 % to 86.13 %. This increase was due to the attachment of DQB on *Chlorella*. These represented that we successfully constructed DQB@C, the microalgae platform improved the stability and dispersibility of DQB self-assemble nanoparticle.

3.7. Hydrogen release and biosafety detection

We also assessed the vivo and vitro biosafety. For vascular endothelial and alveolar epithelium cells, no significant toxicity was found from concentration, 0–100 μg/ml. While, at 20 μg/ml, promoting proliferation effects for two types of cells were both obvious (Fig. 5D). So, following vitro experiments all adopted to this concentration. Vivo biosafety was detected by hemolysis assay. Also, highest concentration to 100 μg/ml, no apparent hemolysis phenomena was observed (Fig. 5E). So, we demonstrated the biosafety and reduction ability of DQB@C. We primarly focused on hydrogen gas release. In Fig. 5F, compared to DQB, DQB@C was of continuous and slow release of hydrogen release in PH 6.8 environment. And at 6 h after CLP operation timepoint, systemic inflammation start to form, we could observe a large amount of molecular hydrogen appeared in organs (Fig. 5G).

3.8. Intracellular absorption and anti oxidative stress detection

In Fig. 5H, we observed two types of cells both within stronger greenish fluorescence at 2 h, 12 h and 24 h after co-culturing with DQB@C. It suggested the DQB@C was of good abilities to enter the cell carrying drugs. Furthermore, we detected the superoxide anion by DHE probes. As shown in Fig. 6A, large amounts of superoxide anion were produced in two types of cells after LPS activation. After riched molecular hydrogen water adding, the intracellular superoxide anion level started to decrease.Compared to hydrogen water, DQB was of better protection ability. While, DQB@C could maximize the effects of preventing intracellular superoxide anion production. Differring from superoxide anion, DCFH-DA detection could indirectly reflect the consumption of GSH. The changes of reactive oxygen species were like superoxide anion (Fig. 6B). DQB@C enabled to decrease the intracellular ROS accumulation induced by LPS. This could prevent excessive consumption of intracelluar GSH.The accumulation of Fe^{2+} was also related to oxidative stress. In Fig. 6C, we could obviously observed fluorescence intensity of intracellular Fe^{2+} was significantly increased. HW and DQB discouraged this accumulation. Interestingly, DQB@C treatment could alomostly restore Fe^{2+} accumulation level to normal level in HUVEC and BEAS-2B. Dihydroquerctin could form complex with Fe^{2+}, it was of better anti oxidative stress and reduce accumulation of Fe^{2+} [38].

Mitochondrial function also was influenced by oxidative stress. In Fig. 6D, LPS could decrease mitochondrial membrane potential. Molecular hydrogen was able to hinder this decrease to a extent. Self-assemble DQB nanoparticles strengthened this effect. What's more important, DQB@C nano system realized protecting mitochondrial against LPS damage.

3.9. Anti-inflammation capability detection

In addition, we observed the inflammatory factor secretory ability of

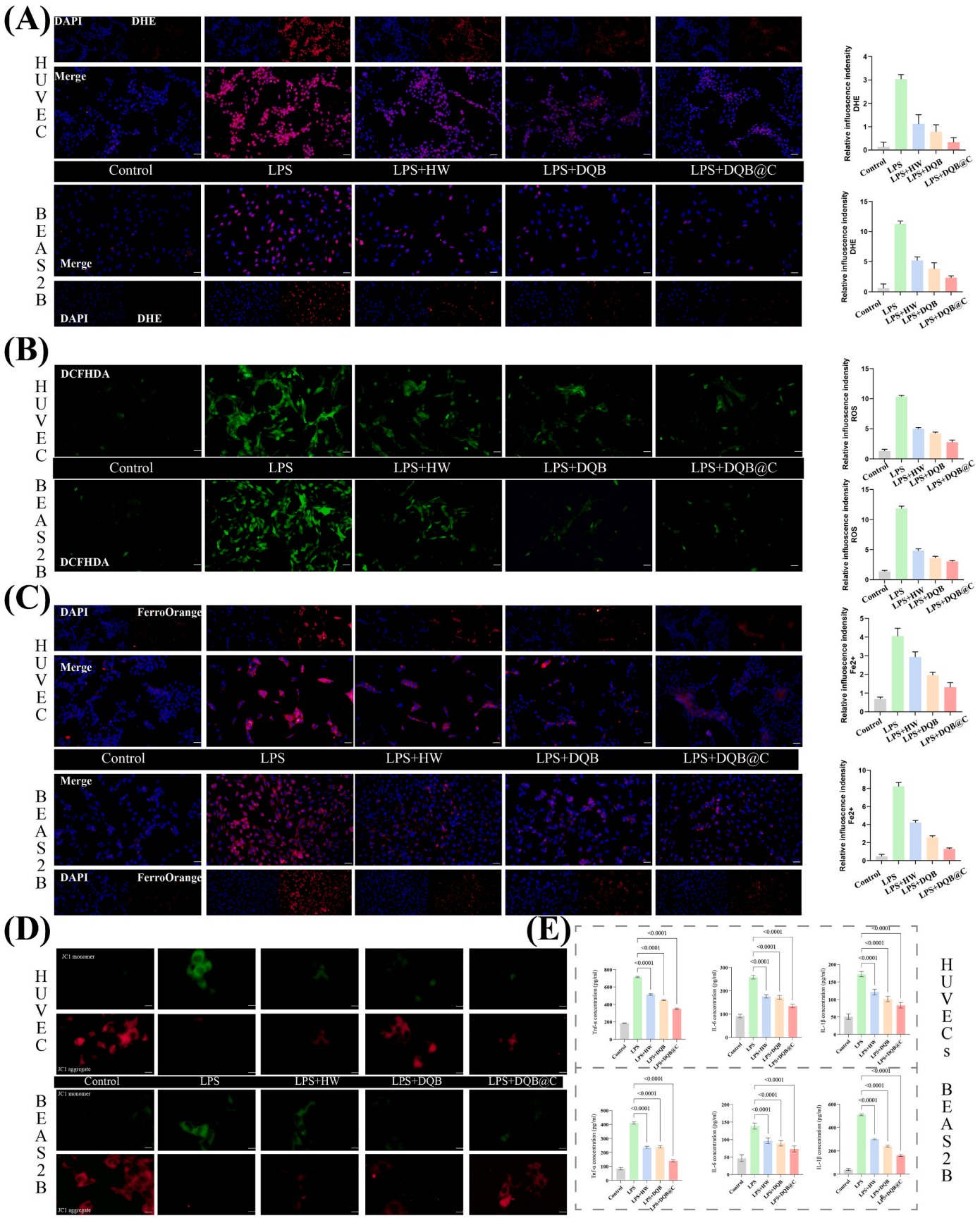

(caption on next page)

Fig. 6. Vitro anti-inflammation and anti-oxidative stress validation. (A) Fluorescent image for DHE straining for two types of cells. Red represented DHE. Blue represented cell nucleus. Histogram was for relative DHE fluorescence intensity. Different color represented different groups. Scale bar, 40 μm. Histogram are expressed with mean ± SD, n = 5. **(B)** Fluorescent image of ROS detection for two types of cells. Green represented reactive oxygen. Histogram was for relative ROS fluorescence intensity. Different colors represented different groups. Scale bar, 40 μm. Histogram are expressed with mean ± SD, n = 5. **(C)** Fluorescent image of intracellular Fe^{2+} distribution. Red represented Fe^{2+} marked by FerroOrange probe. Blue represented cell nucleus. Histogram was for relative Fe^{2+} fluorescence intensity. Scale bar, 40 μm. Histogram are expressed with mean ± SD. (**D**) Fluorescent image of mitochondrial membrane potential. Red represented JC-1 aggregate, green represented JC-1 monomer. Scale bar, 10 μm. Histogram are expressed with mean ± SD, n = 5. **(E)** ELISA results of three inflammation factors. Separate the results of different cells using dashed lines. Histogram are expressed with mean ± SD. Specific *P-value* is annotated on the diagram, n = 5. (For interpretation of the references to colour in this figure legend, the reader is referred to the Web version of this article.)

two cells before and after LPS stimulation and nano system influencing. For endothelial and epithelial cells, IL-6 is the primary secreting factor, thus, detected the expressional level of IL-6 [35]. Meanwhile, we detected Tnf-α and Il-1β level to validate their relationship with Zo-1 and Esam protein. As shown in Fig. 6E, significant increase was observed in IL-6 level after LPS stimulating. Effects of riched molecular hydrogen water enabled to decrease this abnormal change to half of pathogenical state. DQB@C strengthened this positive effects. In HUVECs, DQB@C could decrease Il-6 from 258.4 pg/ml to 134.5 pg/ml. In BEASE-2B, Il-6 decreased from 138.5 pg/ml to 73.5 pg/ml after DQB@C treatment. For two species of cells, changes of Tnf-α and Il-1β level also exhibited similar trends like Il-6. So, synergistic effects of our nano-system in anti-inflammation were proved.

3.10. Vitro anti-ferroptosis and tight junction protection evaluation

For ferroptosis, two proteins (Slc7a11/xCT and Cox2) were detected. For Slc7a11, a protein playing protective roles, LPS stimulation decreased its expression levels in two cell species. DQB@C prevented this decrease and reserved the protein expression level higher than HW (Fig. 7A).

We also observed the changes of Cox2 in cell level. Protein level of two cells both were increased due to the influence of LPS. These induced the iron accumulation and cell damage. These were consistent with what we observed in oxidative stress. As adding riched molecular hydrogen water and DQB, we observed the abnormally protein elevated levels falled back (Fig. 7B). The two proteins, Zo-1 and Esam, were primarily expressed in vascular endothelial cells. So, we focused on the protein level change in HUVEC. We observed that 20 μg/ml DQB and HW were capable of protecting cells against LPS toxiology. Zo-1 protein expression level will increase to 1.5 fold and 2 fold compared to LPS respetively under the HW and DQB influence (Fig. 7C). DQB@C could stengthen this positive effects. Esam protein was of the assemble results. Compared to only molecular hydrogen, DQB@C owned more effective protection effects. These indicated that DQB@C enabled to protect Zo-1 and Esam against inflammation status influence. It maximized the synergistic protective effects of molecular hydrogen and dihydroquercetin in HUVEC.

3.11. Survival rate and vivo anti-inflammation effects evaluation

As shown in Fig. 8A, vivo experiments was performed according to this process. Firstly, we compared mice 24 h survival rate with sham, CLP, CLP + DQB, CLP + DQB@C and CLP + meropenem groups (Fig. 8B). DQB@C was capable of increasing survival rate to 70 % percent which was same as meropenem (40 % in CLP, 50 % CLP + DQB).

Firstly, we evaluated the anti-inflammation effects in vivo. CRP is a direct indicator for evluating inflammation. In Fig. 8C, DQB treatment could not significantly descrease concentration of CRP in serum. While, DQB@C was able to improve the anti-infammation effects of DQB. Effects of DQB@C was close to meropenem. In addition, we evaluated the anti-infection effects, which was also inducer for sepsis in CLP mice. In Fig. 8D, DQB@C could decrease blood bacteria concentrion caused by CLP operation, but its anti-infection effects was not as good as meropenem.

3.12. Vivo organ protection and targeted therapy effects

Metabolic indicators for liver and kideny were indicated. In Fig. 8E, ALT level was decreased after DQB@C treatment. This indicated liver function got restored. For creatinine level, DQB@C treatment group exhibited better ability to clear creatinine than meropenem treatment group. For two lung related indicators, sRAGE and s-PD both could reflect the injury degree of lung. DQB@C also exhibited better protection ability than meropenem in the two indicators.

For H&E staining, five organs all had signs of damage after CLP operation. From Fig. 8F, we could observe the effects of DQB@C treatment including repairing myocardial fibers, relieving alveolar swelling, lesion of damage on liver cells and renal tubular epithelial cells, and restore of spleen marrow structure.

We specially focused on related protein expression changes in lung. In Fig. 8G, Zo-1 and Esam protein changes were consistent. CLP operation enabled to decrease Zo-1 and Esam protein level. DQB will recover these decreases. Intrgrative usage of DQB@C was able to stengthen protective effects compared to only DQB. What's more important, compared to meropenem, DQB@C exhibited better effects on expression level of Zo-1 and Esam. This indicated that DQB@C was capable of targeting tight junction in vivo. To reveal ferroptosis related changes in lung, GSH, MDA and Fe^{2+} concentration were detected.

These three indicators could show the oxidative stress and iron accumulation changes in lung. DQB@C was helpful to eliminate the excessive accumulation of iron ions and increase antioxidants (MDA and GSH) levels (Fig. 8H).

4. Discussion

For severe sepsis patients, approximately 50 % will develop acute lung injury [39],and sepsis induced lung injury has a higher mortality rate compared to other causes of lung injury [40]. In this research, Tjp1-Esam and ferroptosis were identified as potential protein and pathway targets for hydrogen gas treatment. To promote hydrogen gas treatment, nanoalgae system based on self-assemble nanoparticle was constructed. Further experiments validated that nanoalgae system was of capability to integrating hydrogen gas and natural medicine treatment together for preventing acute lung injury.

A large number of proteins are phosphorylated in living organisms [41], which can affect intracellular signal transduction, cell life cycle, metabolic processes, and regulate the adaptability of pathogenic microorganisms, among others [42]. Many studies have shown that some important biomarkers have phosphorylation disorders in diseases such as lung cancer, skin cancer, chronic myeloid leukemia, Alzheimer's disease and diabetes, etc [43,44]. The role of phosphorylated proteomics in revealing the pathogenesis of sepsis and molecular hydrogen treatment has also been reported. For example, hydrogen could alleviate sepsis induced brain injury through phosphorylation mediated PI3K-Art signaling pathway [45]. In sepsis related lung injury, we found significant changes in the expression of Esam and Tjp1 through phosphorylation proteomics analysis. Esam is a phosphorylated kinase, and studies have shown that gene inactivation of Esam enhances the permeability of pulmonary blood vessels, but is not affected by the heart, skin, and brain [46]. Tjp1 is a tight junction protein, which is a substrate of Esam and plays an important role in maintaining vascular integrity [47]. In our

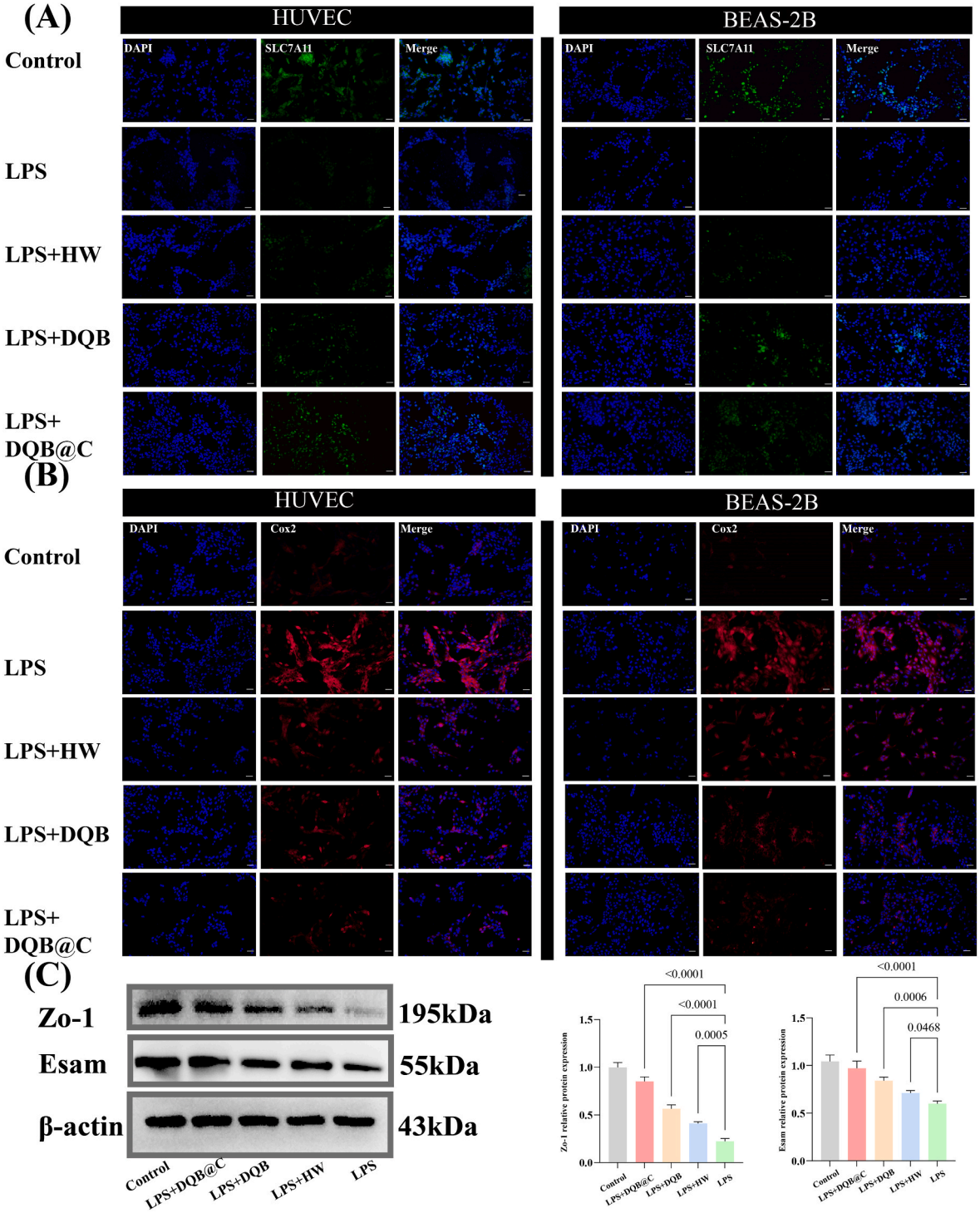

Fig. 7. Results of vitro anti-ferroptosis and tight junction protection. (A) Fluorescent image of intracellular Slc7a11/xCT protein expression level. Green represented Slc7a11, blue represented cell nucleus. Scale bar, 40 μm, n = 5. **(B)** Fluorescent image of intracellular Cox2 protein expression level. Red represented Cox2. blue represented cell nucleus. Scale bar, 40 μm, n = 5. **(C)** Western blot results for Zo-1 and Esam protein in endothelial cell. Histogram are expressed with mean ± SD. Specific *P-value* is annotated on the diagram, n = 3. (For interpretation of the references to colour in this figure legend, the reader is referred to the Web version of this article.)

research, we found that phosphorylation site at S(1)VAS(1)S(1)QPAKPTK of Zo-1 could be high-regulated expression in sepsis. Hydrogen gas treatment on sepsis could make it down-regulated expression. Studies have proved that phosphorylation of Zo-1 could break the tight junction [48]. For Esam, we identified MGAVPVMVPAQS(1)QAGS(1)LV sites, which molecular hydrogen prevent down-regulated expression in sepsis. Esam is kinase for Zo-1. So, its phosphorylation is useful to protect tight junction.

Changes of metabolisms and metabolimics patterns were essenetial for development of acute lung injury [49]. In metabolomics analysis, ferroptosis and glutathione metabolism were proposed at the same time. Srudies have proved that dysfunction of glutathione metabolims played key roles in the occurrence of ferroptosis [50]. Recent studies have shown that ferroptosis plays an important regulatory role in the

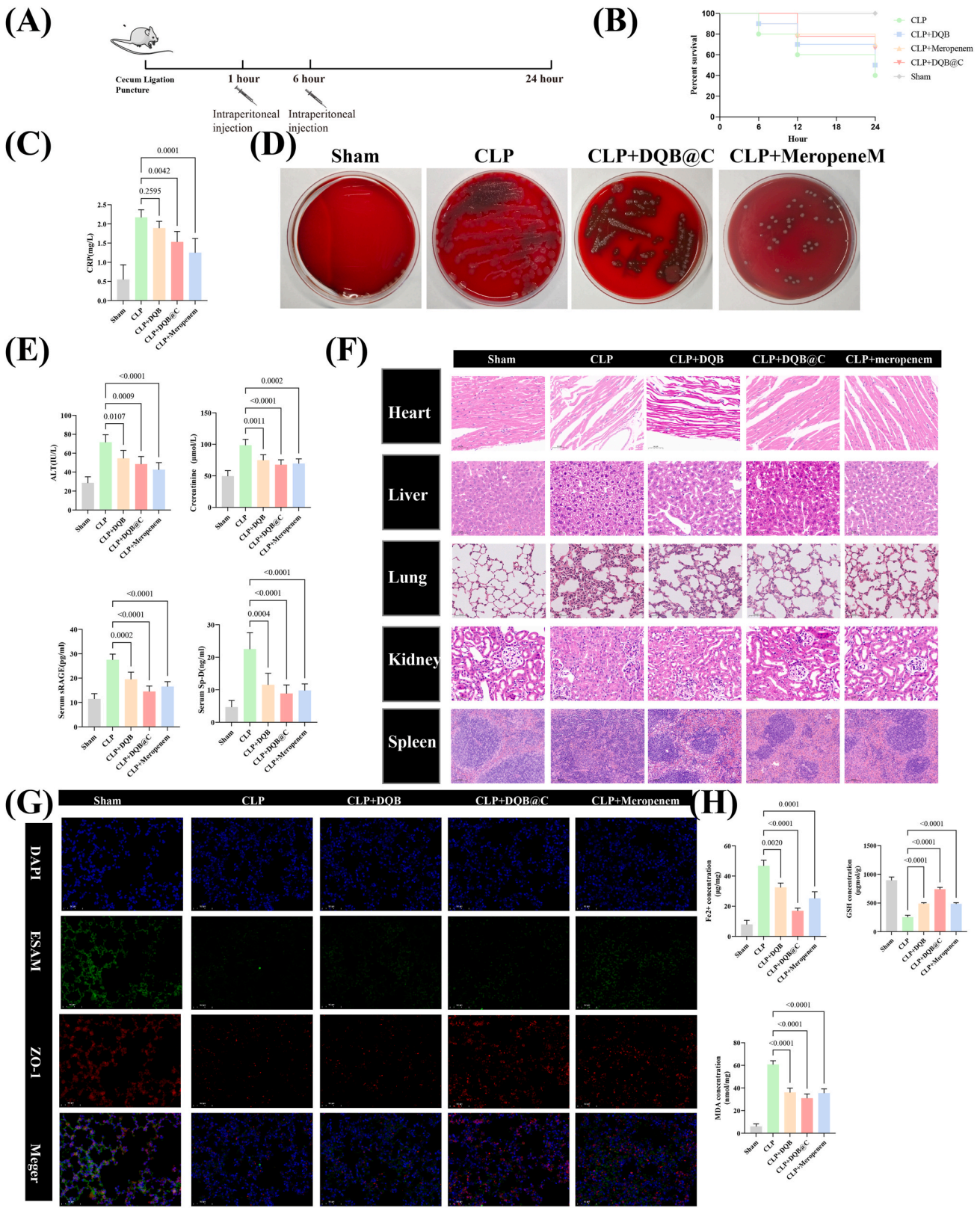

Fig. 8. Vivo anti-ferroptosis and organ protection validation. **(A)** Specific process for vivo experiments. **(B)** Survival rate curve for five groups. Different colors represented different groups. Histogram are expressed with mean ± SD, n = 5. **(C)** Serum CRP level changes in vivo experiments. Histogram are expressed with mean ± SD. Specific *P-value* is annotated on the diagram. n = 5. **(D)** Results of bacterial blood culture from different groups. **(E)** Serum ALT, creatinine, Sp-D and s-RAGE level changes in vivo experiments. Histogram are expressed with mean ± SD. Specific *P-value* is annotated on the diagram, n = 5. **(F)** H&E staining for important organs in vivo experiments. Five organs and five groups were included. Scale bar (heart, liver, lung, kidney), 50 μm. Scale bar (spleen), 100 μm. **(G)** Fluorescent image of Esam and Zo-1 protein colocalization in lung. Green represented Esam, red represented Zo-1. Blue represented cell nucleus. Scale bar, 50 μm, n = 5. **(H)** Results of tissue Fe^{2+}, GSH and MDA concentration in lung. Histogram are expressed with mean ± SD. Specific *P-value* is annotated on the diagram, n = 5. (For interpretation of the references to colour in this figure legend, the reader is referred to the Web version of this article.)

occurrence and development of sepsis [51]. Researchers began to focus on whether targeting ferroptosis can achieve the goal of disease prevention and treatment. A study reported that dihydroquercetin regulated the Nrf2 signaling pathway to inhibit ferroptosis in COPD [52]. So, the two pathways were seen as pathway targets for hydrogen gas in our study.

Dihydroquercetin has strong antioxidant capacity and is widely distributed and rich in content, therefore its medicinal value has been recognized to a certain extent [53]. The latest research indicates that dihydroquercetin improves LPS induced acute lung injury in mice by regulating macrophage M2 polarization [54]. Another study also showed that dihydroquercetin can improve sepsis induced pulmonary capillary leakage [55]. However, due to the poor water solubility of dihydroquercetin [56], and its difficulty in being absorbed. The assemble nano system, DQB@C, utmostly reserved the chemistry characters of dihydroquercetin. In vitro experiments, it exhibited well antioxidants ability and achieved quick intracellular absorbation and release.

We primarily relied on hydrogen production ability of ammonia borane and carrier ability of Chlorella pyrenoidosa to achieve infection-repsonsive hydrogen release. Many studies have confirmed the protective effect of hydrogen in various diseases, including sepsis [57],and the current administration methods are mostly hydrogen inhalation and hydrogen rich water gavage [58,59]. One study developed a biodegradable Tobramycin loaded magnesium micro motor (Mg-Tob motor) as a potential hydrogen generator and active antibiotic delivery agent for synergistic treatment of sepsis, significantly improving the survival rate of sepsis patients [60]. While, metal nanaoparticles could bring biosafety problems [61]. Being different from previous studies which embedded microalgae with cationic polymers [62], DQB@C nano system was one dynamicaly stable system. The development of sepsis in CLP model is rapid, thus, the initative absorpation and dynamic attachment in DQB@C system could ensure DQB nanoparticles to quick release hydrogen gas and dihydroquercetin during inflammation. Vitro experiment results showed that vascular endothelial cells and alveolar epithelialg cells both phagocytose nanoalgae carrying self-assembled nanoparticles into the cells, thereby improving the oxidative stress response of cells and increasing the expression levels of Esam and Tjp1.

Further in vivo experiments confirmed the effectiveness of the nanoalgae system. Nanoalgae reduced the systemic inflammatory response, improved survival rate, and regulated tight junctions and ferroptosis of mice.We specially compared the effects of nanoalgae system with meropenem. One previous study developed a silver metal organic framework (AgMOF) nanoparticle to resist bactrials and treat inflammation, also compared with meropenem [63]. According to our experiment data, DQB@C could realize multi-organ protection effects close to meropenem during acute phase of severe sepsis. This is consistent with our research hypothesis, and the nanoalgae we constructed significantly improved the utilization rate of dihydroquercetin.

In terms to anti-infection, DQB@C could inhibit the development of bacteremia possibily due to the protection of tight junction in tissue. While, DQB@C still lacked bactericidal ability similar to meropenem. This will be our future research focus.

5. Conclusions

This research constructed a novel nano system capable of releasing hydrogen gas at infection microenvironment. The self-assemble nanoparticle is of well biosafety the same as hydrogen gas and improves prevention effects on sepsis related acute lung injury.

Funding

This work was funded by Tianjin Key Medical Discipline (Specialty) Construction Project, (TJYXZDXK-036A), sponsored by Tianjin Health Research Project (TJWJ2022XK006).

Consent for publication

Not applicable.

Ethics approval and consent to participate

This study was approved by Ethics Committee of Tianjin Medical University (IRB2021-DWFL-352). Moreover, the experiments were designed, performed, and reported according to the Animal Research Reporting of In Vivo Experiments (ARRIVE) guidelines [1].

CRediT authorship contribution statement

Yuanlin Wang: Writing – original draft, Methodology, Data curation. **Qingqing Han:** Writing – original draft, Visualization, Validation. **Lingling Liu:** Writing – original draft, Resources, Methodology. **Shuai Wang:** Methodology, Formal analysis, Data curation. **Yongfa Li:** Visualization, Validation, Software. **Zhanying Qian:** Data curation, Conceptualization. **Yi Jiang:** Writing – review & editing, Supervision. **Yonghao Yu:** Writing – review & editing, Funding acquisition.

Declaration of competing interest

No conflict of interest exits in the submission of this manuscript, and manuscript is approved by all authors for publication. I would like to declare on behalf of my co-authors that the work described was original research that has not been published previously. All the authors listed have approved the manuscript that is enclosed.

Data availability

Data will be made available on request.

Acknowledgements

This work was funded by Tianjin Key Medical Discipline (Specialty) Construction Project, (TJYXZDXK-036A), sponsored by Tianjin Health Research Project (TJWJ2022XK006). This study was approved by Ethics Committee of Tianjin Medical University (IRB2022-DW-65). Moreover, the experiments were designed, performed, and reported according to the Animal Research Reporting of In Vivo Experiments (ARRIVE) guidelines [1].

Appendix A. Supplementary data

Supplementary data to this article can be found online at https://doi.org/10.1016/j.mtbio.2024.101247.

References

[1] C. Kilkenny, W. Browne, I.C. Cuthill, M. Emerson, D.G. Altman, Animal research: reporting in vivo experiments: the ARRIVE guidelines, Br. J. Pharmacol. 160 (2010) 1577–1579, https://doi.org/10.1111/j.1476-5381.2010.00872.x.

[2] K.E. Rudd, S.C. Johnson, K.M. Agesa, K.A. Shackelford, D. Tsoi, et al., Global, regional, and national sepsis incidence and mortality, 1990-2017: analysis for the Global Burden of Disease Study, Lancet (London, England) 395 (2020) 200–211, https://doi.org/10.1016/s0140-6736(19)32989-7.

[3] M. Singer, C.S. Deutschman, C.W. Seymour, M. Shankar-Hari, D. Annane, et al., The third international consensus definitions for sepsis and septic shock (Sepsis-3), JAMA 315 (2016) 801–810, https://doi.org/10.1001/jama.2016.0287.

[4] L. Evans, A. Rhodes, W. Alhazzani, M. Antonelli, C.M. Coopersmith, et al., Surviving sepsis campaign: international guidelines for management of sepsis and septic shock 2021, Intensive Care Med. 47 (2021) 1181–1247, https://doi.org/10.1007/s00134-021-06506-y.

[5] J. Li, X. Chen, F. Yang, Advances in the methods of phosphopeptide enrichment and separation in phosphoproteomic research], Sheng wu gong cheng xue bao = Chinese journal of biotechnology 38 (2022) 3648–3658, https://doi.org/10.13345/j.cjb.220599.

[6] L. Huang, J. Chen, X. Li, M. Huang, J. Liu, et al., Polydatin improves sepsis-associated encephalopathy by activating Sirt1 and reducing p38 phosphorylation, J. Surg. Res. 276 (2022) 379–393, https://doi.org/10.1016/j.jss.2022.03.008.

[7] F. Zhang, L. Qi, Q. Feng, B. Zhang, X. Li, et al., HIPK2 phosphorylates HDAC3 for NF-κB acetylation to ameliorate colitis-associated colorectal carcinoma and sepsis, Proc Natl Acad Sci U S A 118 (2021), https://doi.org/10.1073/pnas.2021798118.
[8] Z. Li, M. Gao, B. Yang, H. Zhang, K. Wang, et al., Naringin attenuates MLC phosphorylation and NF-κB activation to protect sepsis-induced intestinal injury via RhoA/ROCK pathway, Biomedicine & pharmacotherapy = Biomedecine & pharmacotherapie 103 (2018) 50–58, https://doi.org/10.1016/j.biopha.2018.03.163.
[9] D. Janosevic, J. Myslinski, T.W. McCarthy, A. Zollman, F. Syed, et al., The orchestrated cellular and molecular responses of the kidney to endotoxin define a precise sepsis timeline, Elife 10 (2021), https://doi.org/10.7554/eLife.62270.
[10] H.H. Yang, J.X. Duan, S.K. Liu, J.B. Xiong, X.X. Guan, et al., A COX-2/sEH dual inhibitor PTUPB alleviates lipopolysaccharide-induced acute lung injury in mice by inhibiting NLRP3 inflammasome activation, Theranostics 10 (2020) 4749–4761, https://doi.org/10.7150/thno.43108.
[11] T. Wang, M. Yegambaram, C. Gross, X. Sun, Q. Lu, et al., RAC1 nitration at Y(32) IS involved in the endothelial barrier disruption associated with lipopolysaccharide-mediated acute lung injury, Redox Biol. 38 (2021) 101794, https://doi.org/10.1016/j.redox.2020.101794.
[12] X.T. Huang, W. Liu, Y. Zhou, M. Sun, H.H. Yang, et al., Galectin-1 ameliorates lipopolysaccharide-induced acute lung injury via AMPK-Nrf2 pathway in mice, Free radical biology & medicine 146 (2020) 222–233, https://doi.org/10.1016/j.freeradbiomed.2019.11.011.
[13] F. Cao, S.-Y. Gui, X. Gao, W. Zhang, Z.-Y. Fu, et al., Research progress of natural product-based nanomaterials for the treatment of inflammation-related diseases, Mater. Des. 218 (2022), https://doi.org/10.1016/j.matdes.2022.110686.
[14] Y. Cui, W. Zhang, J. Shan, J. He, Q. Niu, et al., Copper nanodots-based hybrid hydrogels with multiple enzyme activities for acute and infected wound repair, Adv Healthc Mater 13 (2024) e2302566, https://doi.org/10.1002/adhm.202302566.
[15] S. Gui, W. Tang, Z. Huang, X. Wang, S. Gui, et al., Ultrasmall coordination polymer nanodots Fe-quer nanozymes for preventing and delaying the development and progression of diabetic retinopathy, Adv. Funct. Mater. 36/2023). Advanced Functional Materials 33 (2023) 2370213, https://doi.org/10.1002/adfm.202370213.
[16] A. Dong, Y. Yu, Y. Wang, C. Li, H. Chen, et al., Protective effects of hydrogen gas against sepsis-induced acute lung injury via regulation of mitochondrial function and dynamics, Int. Immunopharm. 65 (2018) 366–372, https://doi.org/10.1016/j.intimp.2018.10.012.
[17] Y. Yu, Y. Yang, M. Yang, C. Wang, K. Xie, et al., Hydrogen gas reduces HMGB1 release in lung tissues of septic mice in an Nrf2/HO-1-dependent pathway, Int. Immunopharm. 69 (2019) 11–18, https://doi.org/10.1016/j.intimp.2019.01.022.
[18] H. Wang, X. Fan, Y. Zhang, D. Yang, R. Guo, Sustained photo-hydrogen production by Chlorella pyrenoidosa without sulfur depletion, Biotechnol. Lett. 33 (2011) 1345–1350, https://doi.org/10.1007/s10529-011-0584-x.
[19] R.L. Hawkins, M. Nakamura, Expression of human growth hormone by the eukaryotic alga, Chlorella, Curr. Microbiol. 38 (1999) 335–341, https://doi.org/10.1007/pl00006813.
[20] D.H. Kim, Y.T. Kim, J.J. Cho, J.H. Bae, S.B. Hur, et al., Stable integration and functional expression of flounder growth hormone gene in transformed microalga, Chlorella ellipsoidea, Mar. Biotechnol. 4 (2002) 63–73, https://doi.org/10.1007/s1012601-0070-x.
[21] J. Zhang, Q. Hao, L. Bai, J. Xu, W. Yin, et al., Overexpression of the soybean transcription factor GmDof4 significantly enhances the lipid content of Chlorella ellipsoidea, Biotechnol. Biofuels 7 (2014) 128, https://doi.org/10.1186/s13068-014-0128-4.
[22] D. Zhong, K. Jin, R. Wang, B. Chen, J. Zhang, et al., Microalgae-based hydrogel for inflammatory bowel disease and its associated anxiety and depression, Advanced materials (Deerfield Beach, Fla) 36 (2024) e2312275, https://doi.org/10.1002/adma.202312275.
[23] D. Zhang, D. Zhong, J. Ouyang, J. He, Y. Qi, et al., Microalgae-based oral microcarriers for gut microbiota homeostasis and intestinal protection in cancer radiotherapy, Nat. Commun. 13 (2022) 1413, https://doi.org/10.1038/s41467-022-28744-4.
[24] S. Guan, Z. Yuan, S. Zhao, Z. Zhuang, H. Zhang, et al., Efficient hydrogen generation from ammonia borane hydrolysis on a tandem ruthenium-platinum-titanium catalyst, Angew. Chem. 63 (2024) e202408193, https://doi.org/10.1002/anie.202408193.
[25] Z. Jin, Y. Sun, T. Yang, L. Tan, P. Lv, et al., Nanocapsule-mediated sustained H(2) release in the gut ameliorates metabolic dysfunction-associated fatty liver disease, Biomaterials 276 (2021) 121030, https://doi.org/10.1016/j.biomaterials.2021.121030.
[26] L. Bai, W. Yi, Y. Wang, Y. Tian, B. Zhou, et al., A PdMo bimetallene with precise wavelength adjustment and catalysis for synergistic photothermal ablation and hydrogen therapy of cancer at different depths, J. Mater. Chem. B 9 (2021) 6441–6459, https://doi.org/10.1039/d1tb01284c.
[27] W. He, D. Fu, Y. Gai, X. Liu, C. Yang, et al., An infection-microenvironment-targeted and responsive peptide-drug nanosystem for sepsis emergency by suppressing infection and inflammation, Asian J. Pharm. Sci. 18 (2023) 100869, https://doi.org/10.1016/j.ajps.2023.100869.
[28] K. Xie, Y. Yu, Y. Pei, L. Hou, S. Chen, et al., Protective effects of hydrogen gas on murine polymicrobial sepsis via reducing oxidative stress and HMGB1 release, Shock 34 (2010) 90–97, https://doi.org/10.1097/SHK.0b013e3181cdc4ae.
[29] C. Hu, T. Li, Y. Xu, X. Zhang, F. Li, et al., CellMarker 2.0: an updated database of manually curated cell markers in human/mouse and web tools based on scRNA-seq data, Nucleic acids research 51 (2022) D870–D876, https://doi.org/10.1093/nar/gkac947%JNucleicAcidsResearch.
[30] S. Fang, L. Dong, L. Liu, J. Guo, L. Zhao, et al., HERB: a high-throughput experiment- and reference-guided database of traditional Chinese medicine, Nucleic acids research 49 (2021) D1197–d1206, https://doi.org/10.1093/nar/gkaa1063.
[31] Z.Y. Liu, N.H. Meng, P.P. Cao, F.P. Peng, J.Y. Luo, et al., Detection of myeloma cell-derived microvesicles: a tool to monitor multiple myeloma load, Exp. Hematol. Oncol. 12 (2023) 26, https://doi.org/10.1186/s40164-023-00392-4.
[32] Z.Y. Liu, M.Y. Tian, L. Deng, Y.S. Wang, R. Xing, et al., The potential diagnostic power of CD138+ microparticles from the plasma analysis for multiple myeloma clinical monitoring, Hematol. Oncol. 37 (2019) 401–408, https://doi.org/10.1002/hon.2648.
[33] M. Yan, Y. Yu, X. Mao, J. Feng, Y. Wang, et al., Hydrogen gas inhalation attenuates sepsis-induced liver injury in a FUNDC1-dependent manner, Int. Immunopharm. 71 (2019) 61–67, https://doi.org/10.1016/j.intimp.2019.03.021.
[34] Y. Yu, X. Ma, T. Yang, B. Li, K. Xie, et al., Protective effect of hydrogen-rich medium against high glucose-induced apoptosis of Schwann cells in vitro, Mol. Med. Rep. 12 (2015) 3986–3992, https://doi.org/10.3892/mmr.2015.3874.
[35] S. Kang, S. Onishi, Z. Ling, H. Inoue, Y. Zhang, et al., Gp130-HIF1α axis-induced vascular damage is prevented by the short-term inhibition of IL-6 receptor signaling, Proceedings of the National Academy of Sciences of the United States of America 121 (2024) e2315898120, https://doi.org/10.1073/pnas.2315898120.
[36] J. Zhang, X. Zhang, J. Li, Z. Song, Systematic analysis of the ABC transporter family in hepatocellular carcinoma reveals the importance of ABCB6 in regulating ferroptosis, Life Sci. 257 (2020) 118131, https://doi.org/10.1016/j.lfs.2020.118131.
[37] Y. Bian, C. Qin, Y. Xin, Y. Yu, H. Chen, et al., Itraq-based quantitative proteomic analysis of lungs in murine polymicrobial sepsis with hydrogen gas treatment, Shock 49 (2018) 187–195, https://doi.org/10.1097/shk.0000000000000927.
[38] V.A. Kostyuk, A.I. Potapovich, E.N. Vladykovskaya, Korkina LG and Afanas'ev IB: influence of metal ions on flavonoid protection against asbestos-induced cell injury, Arch. Biochem. Biophys. 385 (2001) 129–137, https://doi.org/10.1006/abbi.2000.2118.
[39] J.E. Sevransky, M.M. Levy, J.J. Marini, Mechanical ventilation in sepsis-induced acute lung injury/acute respiratory distress syndrome: an evidence-based review, Crit. Care Med. 32 (2004) S548–S553, https://doi.org/10.1097/01.ccm.0000145947.19077.25.
[40] R.D. Stapleton, B.M. Wang, L.D. Hudson, G.D. Rubenfeld, E.S. Caldwell, et al., Causes and timing of death in patients with ARDS, Chest 128 (2005) 525–532, https://doi.org/10.1378/chest.128.2.525.
[41] J.V. Olsen, M. Vermeulen, A. Santamaria, C. Kumar, M.L. Miller, et al., Quantitative phosphoproteomics reveals widespread full phosphorylation site occupancy during mitosis, Sci. Signal. 3 (2010) ra3, https://doi.org/10.1126/scisignal.2000475.
[42] F. Ardito, M. Giuliani, D. Perrone, G. Troiano, L. Lo Muzio, The crucial role of protein phosphorylation in cell signaling and its use as targeted therapy, Int. J. Mol. Med. 40 (2017) 271–280, https://doi.org/10.3892/ijmm.2017.3036 (Review).
[43] E.J. Needham, B.L. Parker, T. Burykin, D.E. James, S.J. Humphrey, Illuminating the dark phosphoproteome, Sci. Signal. 12 (2019), https://doi.org/10.1126/scisignal.aau8645.
[44] H.C. Harsha, A. Pandey, Phosphoproteomics in cancer, Mol. Oncol. 4 (2010) 482–495, https://doi.org/10.1016/j.molonc.2010.09.004.
[45] Y. Bai, L. Li, B. Dong, W. Ma, H. Chen, et al., Phosphorylation-mediated PI3K-Art signalling pathway as a therapeutic mechanism in the hydrogen-induced alleviation of brain injury in septic mice, J. Cell Mol. Med. 26 (2022) 5713–5727, https://doi.org/10.1111/jcmm.17568.
[46] C.N. Duong, A.F. Nottebaum, S. Butz, S. Volkery, D. Zeuschner, et al., Interference with ESAM (endothelial cell-selective adhesion molecule) plus vascular endothelial-cadherin causes immediate lethality and lung-specific blood coagulation, Arterioscler. Thromb. Vasc. Biol. 40 (2020) 378–393, https://doi.org/10.1161/atvbaha.119.313545.
[47] Y. Fouani, L. Kirchhof, L. Stanicek, G. Luxán, A.W. Heumüller, et al., The splicing-regulatory lncRNA NTRAS sustains vascular integrity, EMBO Rep. 23 (2022) e54157, https://doi.org/10.15252/embr.202154157.
[48] O. Beutel, R. Maraspini, K. Pombo-García, C. Martin-Lemaitre, A. Honigmann, Phase separation of zonula occludens proteins drives formation of tight junctions, Cell 179 (2019) 923–936.e911, https://doi.org/10.1016/j.cell.2019.10.011.
[49] M. Pourfathi, S.J. Kadlecek, S. Chatterjee, R.R. Rizi, Metabolic imaging and biological assessment: platforms to evaluate acute lung injury and inflammation, Front. Physiol. 11 (2020) 937, https://doi.org/10.3389/fphys.2020.00937.
[50] J. Fujii, H. Imai, Oxidative metabolism as a cause of lipid peroxidation in the execution of ferroptosis, Int. J. Mol. Sci. 25 (2024), https://doi.org/10.3390/ijms25147544.
[51] L. Xl, Z. Gy, G. R, C. N, Ferroptosis in sepsis: the mechanism, the role and the therapeutic potential, Front. Immunol. 13 (2022) 956361, https://doi.org/10.3389/fimmu.2022.956361.
[52] X. Liu, Y. Ma, L. Luo, D. Zong, H. Li, et al., Dihydroquercetin suppresses cigarette smoke induced ferroptosis in the pathogenesis of chronic obstructive pulmonary disease by activating Nrf2-mediated pathway, Phytomedicine : international journal of phytotherapy and phytopharmacology 96 (2022) 153894, https://doi.org/10.1016/j.phymed.2021.153894.
[53] A.E. Weidmann, Dihydroquercetin: more than just an impurity? Eur. J. Pharmacol. 684 (2012) 19–26, https://doi.org/10.1016/j.ejphar.2012.03.035.

[54] C. Li, J. Liu, C. Zhang, L. Cao, F. Zou, et al., Dihydroquercetin (DHQ) ameliorates LPS-induced acute lung injury by regulating macrophage M2 polarization through IRF4/miR-132-3p/FBXW7 axis, Pulm. Pharmacol. Therapeut. 83 (2023) 102249, https://doi.org/10.1016/j.pupt.2023.102249.
[55] M. Shen, B. Lin, F. Qian, L. Zhao, Y. Xi, et al., Taxifolin ameliorates sepsis-induced lung capillary leak through inhibiting the JAK/STAT3 pathway, Allergol. Immunopathol. 50 (2022) 7–15, https://doi.org/10.15586/aei.v50i2.550.
[56] A.N. Shikov, O.N. Pozharitskaya, I. Miroshnyk, S. Mirza, I.N. Urakova, et al., Nanodispersions of taxifolin: impact of solid-state properties on dissolution behavior, International journal of pharmaceutics 377 (2009) 148–152, https://doi.org/10.1016/j.ijpharm.2009.04.044.
[57] B. Qi, Y. Yu, Y. Wang, Y. Wang, Y. Yu, et al., Perspective of molecular hydrogen in the treatment of sepsis, Curr. Pharmaceut. Des. 27 (2021) 667–678, https://doi.org/10.2174/1381612826666200909124936.
[58] J.S. Dumbuya, S. Li, L. Liang, Y. Chen, J. Du, et al., Effects of hydrogen-rich saline in neuroinflammation and mitochondrial dysfunction in rat model of sepsis-associated encephalopathy, J. Transl. Med. 20 (2022) 546, https://doi.org/10.1186/s12967-022-03746-4.
[59] H. Chen, H. Lin, B. Dong, Y. Wang, Y. Yu, et al., Hydrogen alleviates cell damage and acute lung injury in sepsis via PINK1/Parkin-mediated mitophagy, Inflamm. Res. : official journal of the European Histamine Research Society [et al] 70 (2021) 915–930, https://doi.org/10.1007/s00011-021-01481-y.
[60] Y. Song, R. Zhang, H. Qin, W. Xu, J. Sun, et al., Micromotor-enabled active hydrogen and Tobramycin delivery for synergistic sepsis therapy, Adv. Sci. 10 (2023) e2303759, https://doi.org/10.1002/advs.202303759.
[61] T.T. Truong, S. Mondal, V.H.M. Doan, S. Tak, J. Choi, et al., Precision-engineered metal and metal-oxide nanoparticles for biomedical imaging and healthcare applications, Adv. Colloid Interface Sci. 332 (2024) 103263, https://doi.org/10.1016/j.cis.2024.103263.
[62] C. Ren, D. Zhong, Y. Qi, C. Liu, X. Liu, et al., Bioinspired pH-responsive microalgal hydrogels for oral insulin delivery with both hypoglycemic and insulin sensitizing effects, ACS Nano 17 (2023) 14161–14175, https://doi.org/10.1021/acsnano.3c04897.
[63] L. Lu, L. Quan, J. Li, J. Yuan, X. Nie, et al., Bioengineered stem cell membrane functionalized nanoparticles combine anti-inflammatory and antimicrobial properties for sepsis treatment, J. Nanobiotechnol. 21 (2023) 170, https://doi.org/10.1186/s12951-023-01913-3.